Journal of Materials Chemistry

Cite this: *J. Mater. Chem.*, 2012, **22**, 20210

www.rsc.org/materials

PAPER

Crystal structure of blue–white–yellow color-tunable $Ca_4Si_2O_7F_2$:Eu^{2+},Mn^{2+} phosphor and investigation of color tunability through energy transfer for single-phase white-light near-ultraviolet LEDs†

Chien-Hao Huang,*[ad] Ting-Shan Chan,[b] Wei-Ren Liu,[c] De-Yin Wang,[d] Yi-Chen Chiu,[a] Yao-Tsung Yeh[a] and Teng-Ming Chen*[d]

Received 18th May 2012, Accepted 25th July 2012
DOI: 10.1039/c2jm33160h

The crystal structure of $Ca_4Si_2O_7F_2$:Eu^{2+},Mn^{2+} was refined and determined from X-ray diffraction (XRD) profiles obtained using a synchrotron light source by the Rietveld refinement method. It was found to crystallize into a monoclinic structure with the $P2_1/c$(14) space group. On examining the Mn^{2+}-concentration-dependent photoluminescence properties, we found that the emission colors could be tuned from blue (0.152, 0.112) to white-light (0.351, 0.332) and eventually to yellow (0.430, 0.423) through energy transfer by changing the Eu^{2+}/Mn^{2+} ratio. Moreover, energy transfer from a sensitizer Eu^{2+} to an activator Mn^{2+} occurs *via* a resonance-type dipole–quadrupole interaction mechanism, and the critical distances of the energy transfer were calculated to be 11.66 Å and 12.61 Å using concentration quenching and spectral overlap methods, respectively. Combining a 400 nm near-ultraviolet (NUV) chip and a single-phase white-emitting $(Ca_{0.96}Eu_{0.01}Mn_{0.03})_4Si_2O_7F_2$ phosphor produced a white-light NUV LED with CIE chromaticity coordinates of (0.347, 0.338) and a warm color temperature of 4880 K.

1. Introduction

In recent years, phosphor-converted white light-emitting diodes (LEDs) have been in high demand for use in solid-state lighting technology applications, because of their high efficiency, good material stability, long operational lifetime, and environmentally friendly characteristics.[1–3] Nowadays, the majority of white LEDs use a combination of a blue InGaN chip and a yellow-emitting $Y_3Al_5O_{12}$:Ce^{3+} phosphor. However, the disadvantages of this method are low color-rendering index and high correlated color temperature (CCT). These disadvantages can be attributed to the deficiency of red emission in the visible spectrum.[4] It is also possible to produce white-light by means of adopting two, three, or even four phosphors in near-ultraviolet (NUV)/UV LED chips;[5] however, poor luminous efficiency attributed to reabsorption has commonly been encountered. Thus, white LEDs fabricated using NUV/UV LED chips with a single-composition phosphor are considered to be potentially useful because they exhibit low color aberration, low cost, high color-rendering indexes, good color tone, and tunability of the CIE color coordinates and the CCT. A single-composition white-light phosphor can be produced by co-doping a sensitizer and an activator into the same crystalline matrix, using the principle of energy transfer from the sensitizer to the activator. Mn^{2+}-doped luminescent materials have been known to have wide-range emissions from 500 to 700 nm depending on the crystal field of the host material.[6–8] They could be good candidates from green (weak crystal field) to red (stronger crystal field) phosphors, but the disadvantage of the Mn^{2+} ions is that their d–d absorption transition is difficult to pump, since it is both parity and spin forbidden. As a promising sensitizer for the Mn^{2+} ion, Eu^{2+} has been widely applied in many Mn^{2+}-doped hosts, such as $Ca_9Y(PO_4)_7$,[9] $Ba_3MgSi_2O_8$,[10] $Na(Sr,Ba)PO_4$,[11] $Ca_3Al_2Si_2O_8Cl_4$,[12] $SrMgB_6O_{11}$,[13] $Ca_2SiO_3Cl_2$,[14] $Sr_3Y(PO_4)_3$ (ref. 15) and $Ca_9Gd(PO_4)_7$,[16] to improve the emission intensity of Mn^{2+}.

In this work, we report the preparation and investigation of a series of single-composition emission-tunable $Ca_4Si_2O_7F_2$:Eu^{2+},Mn^{2+} phosphors, including their crystal structure, reflectance spectra, and luminescence properties. The energy transfer mechanism between Eu^{2+} and Mn^{2+} in the $Ca_4Si_2O_7F_2$ host matrix was also studied, and the critical distance of the energy transfer from the sensitizer Eu^{2+} to the activator Mn^{2+}

[a]*Material and Chemical Research Laboratories, Industrial Technology Research Institute, Hsinchu, Taiwan 30011, R.O.C. E-mail: Chien-Hao@itri.org.tw; Tel: +86-886-3-5732438*
[b]*National Synchrotron Radiation Research Center, Hsinchu Science Park, Hsinchu, Taiwan 30076, R.O.C*
[c]*Department of Chemical Engineering, Chung Yuan Christian University, Chungli, Taiwan 32023, R.O.C*
[d]*Phosphors Research Laboratory and Department of Applied Chemistry, National Chiao Tung University, Hsinchu, Taiwan 30010, R.O.C. E-mail: tmchen@mail.nctu.edu.tw; Tel: +86-886-35731695*
† Electronic supplementary information (ESI) available. CCDC 883884. For ESI and crystallographic data in CIF or other electronic format see DOI: 10.1039/c2jm33160h

was calculated by concentration quenching and spectra overlap methods. Finally, we have also successfully demonstrated the fabrication and examined the optical properties of a white phosphor-converted LED by adopting a white-emitting $Ca_4Si_2O_7F_2$:Eu^{2+},Mn^{2+} phosphor with a 400 nm NUV LED chip.

2. Experimental

2.1. Materials and synthesis

A series of rare earth-doped $(Ca_{0.99-x}Eu_{0.01}Mn_x)_4Si_2O_7F_2$ (x = 0–0.1 mol) phosphors were synthesized by a high-temperature solid-state reaction in which the constituent raw materials $CaCO_3$ (99.99%, Aldrich), CaF_2 (99.99%, Aldrich), SiO_2 (99.6%, Aldrich), EuF_2 (99.9%, Alfa) and MnO (99.9%, Aldrich) were weighed in stoichiometric proportions. The powder reactants were blended and ground thoroughly in an agate mortar, and the homogeneous mixture was transferred to an alumina crucible and calcined in a furnace at 1373 K for 8 h under a reducing atmosphere of 15% H_2/85% N_2. The products were then cooled to room temperature in the furnace, ground, and pulverized for further measurements.

2.2. Materials characterization

The crystal structure of the as-synthesized samples identified by using synchrotron XRD patterns with λ = 0.774908 Å (16 keV) were recorded with a large Debye–Scherrer camera installed at beam line 01C2 of the National Synchrotron Radiation Research Center (NSRRC) in Taiwan; the GSAS program[17] was used for the structural refinements. The diffuse reflectance (DR) spectra were measured with a Hitachi 3010 double-beam UV-vis spectrometer (Hitachi Co., Tokyo, Japan). The photoluminescence (PL) and photoluminescence excitation (PLE) spectra of the samples were analyzed by using a Spex Fluorolog-3 Spectrofluorometer equipped with a 450 W Xe light source. The Commission International de I'Eclairage (CIE) chromaticity coordinates for all samples were measured by a Laiko DT-101 color analyzer equipped with a CCD detector (Laiko Co., Tokyo, Japan). The specification for the 400 nm NUV chip: (AOT Product no: DC0004CAA, Spec: 370U02C, wavelength peak: 395–400 ± 0.6 nm, chip size: 40 × 40 mil^2, forward voltage: 3.8–4.0 ± 0.02 V, power: 10–20 ± 0.21 mW).

3. Results and discussion

3.1. Crystal structure

Fig. 1 shows the observed (crosses) and calculated (solid line) synchrotron X-ray diffraction (XRD) profiles and their difference (bottom) for the Rietveld refinement of $(Ca_{0.99}Eu_{0.01})_4Si_2O_7F_2$ and $(Ca_{0.89}Eu_{0.01}Mn_{0.1})_4Si_2O_7F_2$ at room temperature with λ = 0.774908 Å. These results indicate that when Eu^{2+} or Eu^{2+}/Mn^{2+} is doped in the $Ca_4Si_2O_7F_2$ host, it remains single phased. $Ca_4Si_2O_7F_2$:Eu^{2+},Mn^{2+} crystallizes into a monoclinic structure with the space group $P2_1/c$(14).[18] Fig. 1a shows the results of the Rietveld refinement of the $(Ca_{0.99}Eu_{0.01})_4Si_2O_7F_2$ crystal; the lattice parameters were determined to be a = 7.5624(1) Å, b = 10.5722(2) Å, c = 10.9451(2) Å, β = 109.5984(11)°, V = 824.37(9) $Å^3$, and Z = 4 and the refinement finally converged to R_p = 5.23%, R_{wp} = 7.49% and χ^2 = 1.96 (Table 1). Since Ca^{2+} in the $(Ca_{0.99}Eu_{0.01})_4Si_2O_7F_2$ structure was replaced by a small Mn^{2+} ion, the lattice parameters

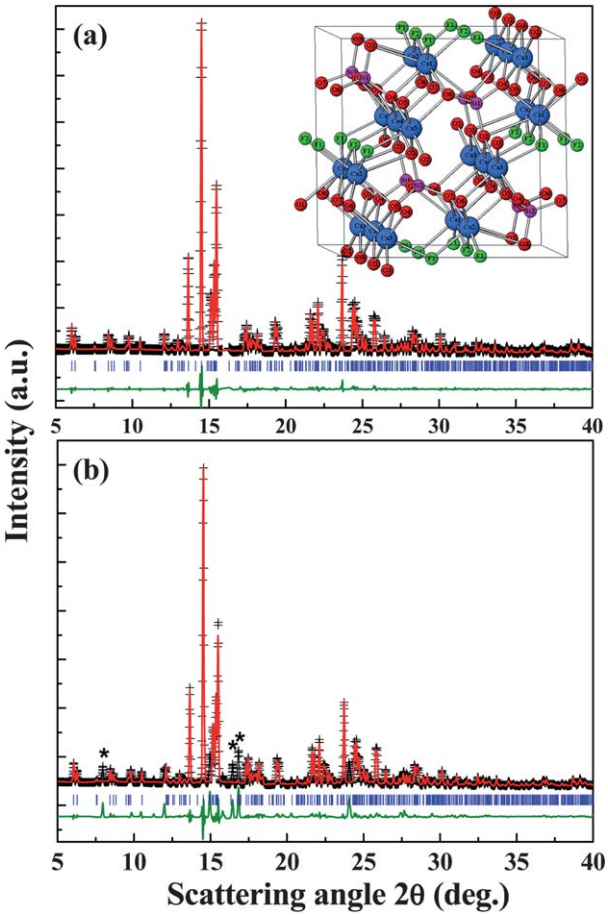

Fig. 1 Observed (crosses) and calculated (solid line) synchrotron XRD profiles and their difference (bottom) for the Rietveld refinement of (a) $(Ca_{0.99}Eu_{0.01})Si_2O_7F_2$ and (b) $(Ca_{0.89}Eu_{0.01}Mn_{0.1})_4Si_2O_7F_2$ at room temperature with λ = 0.774908 Å (16 keV).

Table 1 Rietveld refinement and crystal data of $(Ca_{0.99}Eu_{0.01})_4Si_2O_7F_2$ and $(Ca_{0.89}Eu_{0.01}Mn_{0.1})_4Si_2O_7F_2$ phosphors

Formula	$(Ca_{0.99}Eu_{0.01})_4Si_2O_7F_2$	$(Ca_{0.89}Eu_{0.01}Mn_{0.1})_4Si_2O_7F_2$
Radiation type (Å)	0.7749	0.7749
2θ range (deg.)	5–40	5–40
Temperature (K)	298	298
Formula weight	371.00	376.94
Symmetry	Monoclinic	Monoclinic
Space group	$P2_1/c$(14)	$P2_1/c$(14)
a (Å)	7.5624(1)	7.5463(2)
b (Å)	10.5722(2)	10.5532(4)
c (Å)	10.9451(2)	10.9381(4)
$\alpha = \gamma$ (deg.)	90	90
β (deg.)	109.5984(11)	109.5782(20)
Volume ($Å^3$)	824.37(9)	820.72(5)
Z	4	4
R_p	5.23%	7.05%
R_{wp}	7.49%	10.30%
χ^2	1.96	3.09

of $(Ca_{0.89}Eu_{0.01}Mn_{0.1})_4Si_2O_7F_2$ became $a = 7.5463(2)$ Å, $b = 10.5532(4)$ Å, $c = 10.9381(4)$ Å, $\beta = 109.5782(20)°$, $V = 820.72(5)$ Å^3, and $Z = 4$ and the refinement finally converged to $R_p = 7.05\%$, $R_{wp} = 10.30\%$ and $\chi^2 = 3.09$, in good agreement with the previous result, as shown in Fig. 1b. There is a negligible amount of impurities in phase at $2\theta = 7.96$, 16.43 and 16.82 site, as the $(Ca_{0.99}Eu_{0.01})_4Si_2O_7F_2$ is doped with higher concentrations of Mn^{2+} (>5 mol%). The final refined positions of all atoms and the lattice parameters for the $(Ca_{0.89}Eu_{0.01}Mn_{0.1})_4Si_2O_7F_2$ phosphors are listed in Table S1.†

The insets of Fig. 1a show the crystal structure of $Ca_4Si_2O_7F_2$. Each cation has several different coordination environments: Ca(1) atom is eight-coordinated by five O atoms with an average Ca(1)–O distance of 2.53571 Å and three F atoms with an average Ca(1)–F distance of 2.41412 Å, Ca(2) atom is surrounded by four O and three F atoms at average distances of 2.49490 and 2.33007 Å, Ca(3) atom is six-coordinated by five O atoms at an average Ca(3)–O distance of 2.36809 Å and one F atom at an average Ca(3)–F distance of 2.29127 Å, Ca(4) atoms are seven-coordinated by six O atoms at an average Ca(4)–O distance of 2.45061 Å and one F atom at a Ca(4)–F distance of 2.37536 Å, and Si(1) and Si(2) atoms are tetrahedrally coordinated by four O atoms at average distances of 1.6398 and 1.64253 Å. The bond distance is shown in Table S2.† The ionic radii for the eight- and six-coordinated Ca^{2+} ions are 1.12 and 1.00 Å, respectively. Similarly, the ionic radii for the eight- and six-coordinated Eu^{2+} ions are 1.25 and 1.17 Å and those for Mn^{2+} are 0.96 and 0.83 Å, respectively. Based on the effective ionic radii of cations with different coordination numbers and electric charge balances, we propose that the Eu^{2+} and Mn^{2+} ions are expected to randomly occupy the Ca^{2+} ion sites in the $Ca_4Si_2O_7F_2$ crystal structure.

3.2. Luminescence properties

Fig. 2 illustrates the reflectance spectra of the pure $Ca_4Si_2O_7F_2$ host and Eu^{2+}-doped $Ca_4Si_2O_7F_2$ and the photoluminescence (PL)/photoluminescence excitation (PLE) spectra of the $Ca_4Si_2O_7F_2$:Eu^{2+} phosphors. The reflectance spectrum of the $Ca_4Si_2O_7F_2$ host exhibits an absorption band from 240 to 350 nm that corresponds to the host lattice absorption. The absorption edge of the host material was estimated to be about 4.2 eV (295 nm, 33 898 cm^{-1}).[19,20] Strong absorption occurred in the range from UV to blue (240–500 nm) for the $Ca_4Si_2O_7F_2$:Eu^{2+} matrix, which mainly resulted from the transition of Eu^{2+} from the 4f ground state to a 5d excited state. The PLE spectrum ($\lambda_{em} = 460$ nm) of $Ca_4Si_2O_7F_2$:Eu^{2+} shows a broadband excitation due to the 4f–5d dipole-allowed electronic transitions of Eu^{2+} to an electronic configuration of $4f^65d^1$, which is consistent with the absorption observed in the reflection spectrum. The strong broadband absorption of the $Ca_4Si_2O_7F_2$:Eu^{2+} phosphor matches well with the emission of the NUV chips for applications in white-light NUV LEDs. A broad, asymmetric band was observed in the PL spectrum ($\lambda_{ex} = 400$ nm) of $Ca_4Si_2O_7F_2$:Eu^{2+} in the wavelength range of 420–530 nm with a strong blue emission centered at 460 nm, which corresponds to the allowed $4f^65d^1 \rightarrow 4f^7$ electronic transitions of Eu^{2+} ions.[21] The broad and asymmetric emission bands of $Ca_4Si_2O_7F_2$:Eu^{2+} may be attributed to the transitions of Eu^{2+} ions occupying four crystallographically distinct Ca^{2+} sites in the host structure. The PL spectrum of the $Ca_4Si_2O_7F_2$:Eu^{2+} phosphor can be decomposed by Gaussian deconvolution into four Gaussian profiles with peaks centered at 449 nm (22 272 cm^{-1}), 463 nm (21 598 cm^{-1}), 484 nm (20 661 cm^{-1}), and 513 nm (19 493 cm^{-1}). These peaks can be ascribed to four different emission sites, which could be identified as the four different coordination environments of the Ca^{2+} ion sites occupied by Eu^{2+} ions.

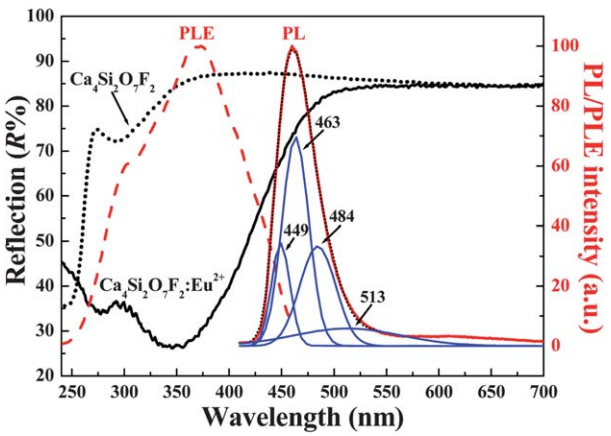

Fig. 2 Reflectance spectra of $Ca_4Si_2O_7F_2$ and $Ca_4Si_2O_7F_2$:Eu^{2+} and PL/PLE spectra of $Ca_4Si_2O_7F_2$:Eu^{2+} phosphor.

The quantum efficiency of a phosphor is an important parameter to be considered for practical applications. To determine the absolute quantum efficiency of photo-conversion for $(Ca_{0.99}Eu_{0.01})_4Si_2O_7F_2$ phosphor, we applied the integrated sphere method for the measurements of optical absorbance (A) and quantum efficiency (Φ) of phosphor samples. The optical absorbance and quantum efficiency were calculated by using the following equations:[22]

$$A = \frac{L_0(\lambda) - L_i(\lambda)}{L_0(\lambda)} \quad (1)$$

$$\Phi = \frac{E_i(\lambda) - (1 - A)\cdot E_0(\lambda)}{L_e(\lambda)\cdot A} \quad (2)$$

where $L_0(\lambda)$ is the integrated excitation profile when the sample is diffusely illuminated by the integrated sphere's surface; $L_i(\lambda)$ is the integrated excitation profile when the sample is directly excited by the incident beam; $E_0(\lambda)$ is the integrated luminescence of the sample excited by indirect illumination from the sphere; and $E_i(\lambda)$ is the integrated luminescence of the sample upon direct excitation. The term $L_e(\lambda)$ is the integrated excitation profile obtained from the empty integrated sphere (without the sample). The internal (η_i) and external (η_o) quantum efficiencies ($A \times \Phi$) were calculated based on the equations previously reported by Hirosaki *et al.*[23] Upon excitation at 400 nm, the optical absorbance (A) of $(Ca_{0.99}Eu_{0.01})_4Si_2O_7F_2$ and $BaMgAl_{10}O_{17}$:Eu^{2+} (BAM:Eu^{2+}) phosphors (commercial product KX661 from Kasei Optonix Ltd) was calculated to be 61.2% and 55.4%, the internal quantum efficiencies were 29.3% and 87.1%, and the corresponding external quantum efficiencies were 17.9% and 48.3%, respectively.

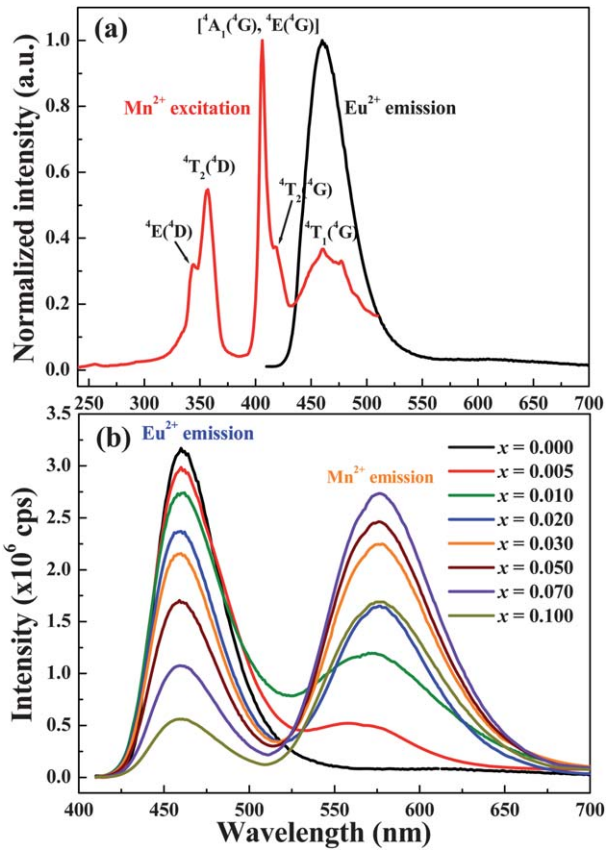

Fig. 3 (a) Spectral overlap between the $Ca_4Si_2O_7F_2$:Eu^{2+} emission spectrum and the $Ca_4Si_2O_7F_2$:Mn^{2+} excitation spectrum and (b) emission spectra of $(Ca_{0.99-x}Eu_{0.01}Mn_x)_4Si_2O_7F_2$ ($x = 0.005$–0.1) phosphors under 400 nm NUV excitation.

As indicated in Fig. 3a, Eu^{2+} of $Ca_4Si_2O_7F_2$:Eu^{2+} shows broadband emission from 420 to 530 nm centered at 460 nm, which was attributed to the $4f^65d^1 \rightarrow 4f^7$ transition. The Mn^{2+} excitation of $Ca_4Si_2O_7F_2$:Mn^{2+}, on the other hand, contains several bands centered at 343, 357, and 461 nm, corresponding to the transitions from the $^6A_1(^6S)$ ground state to the $^4E(^4D)$, $^4T_2(^4D)$, and $^4T_1(^4G)$ excited states, respectively.[24] We have observed significant spectral overlap between the emission band centered at 460 nm of $Ca_4Si_2O_7F_2$:Eu^{2+} and the excitation band centered at 461 nm of $Ca_4Si_2O_7F_2$:Mn^{2+}. Therefore, the spectral overlap is matched for Eu^{2+} and Mn^{2+}, and energy can be transferred from Eu^{2+} to Mn^{2+}. Thus, effective resonance-type energy transfer from a sensitizer Eu^{2+} to an activator Mn^{2+} is expected to occur in $Ca_4Si_2O_7F_2$:Eu^{2+},Mn^{2+}.[25] Fig. 3b shows the emission spectra of $(Ca_{0.99-x}Eu_{0.01}Mn_x)_4Si_2O_7F_2$ phosphors under 400 nm NUV excitation. For $(Ca_{0.99-x}Eu_{0.01}Mn_x)_4Si_2O_7F_2$ samples, two broad emission bands were observed centered at 460 ($4f^65d^1 \rightarrow 4f^7$ transition of Eu^{2+}) and 576 nm ($^4T_1(^4G) \rightarrow {}^6A_1(^6S)$ transition of Mn^{2+}). The emission intensity of Eu^{2+} at 460 nm was found to decrease with increasing Mn^{2+} content x, and the emission intensity of Mn^{2+} at 576 nm was found to increase with increasing Mn^{2+} content until the emission intensity of Mn^{2+} became saturated when x reached 0.1. Concentration quenching occurred when the Mn^{2+} dopant content x was greater than 0.07, which is related to the energy transfer probability from Eu^{2+} to Mn^{2+}. The concentration quenching can be attributed to energy reabsorption among the nearest Eu^{2+} or Mn^{2+} ions.[26]

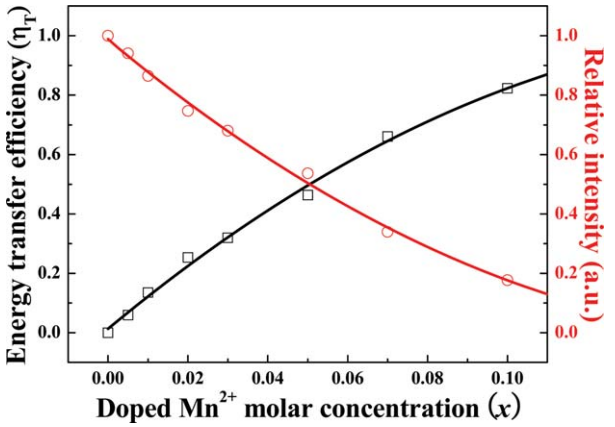

Fig. 4 Energy transfer efficiency η_T and the relative emission intensity of Eu^{2+} as a function of Mn^{2+} molar concentration for $(Ca_{0.99-x}Eu_{0.01}Mn_x)_4Si_2O_7F_2$ ($x = 0$–0.1) phosphors.

Fig. 4 shows the energy transfer efficiency η_T and the relative emission intensity of Eu^{2+} as a function of Mn^{2+} molar concentration for $(Ca_{0.99-x}Eu_{0.01}Mn_x)_4Si_2O_7F_2$ phosphors. The relative emission intensity of Eu^{2+} decreased with increasing Mn^{2+} doping content x in $(Ca_{0.99-x}Eu_{0.01}Mn_x)_4Si_2O_7F_2$ phosphors, and the results indicate continuous energy transfer from the sensitizer Eu^{2+} to the activator Mn^{2+}. According to Paulose *et al.*,[27] the energy transfer efficiency (η_T) from the sensitizer Eu^{2+} to the activator Mn^{2+} can be expressed as

$$\eta_T = 1 - \frac{I_S}{I_{S0}} \quad (3)$$

where I_{S0} is the luminescence intensity of the sensitizer Eu^{2+} in the sample in the absence of Mn^{2+}, and I_S is the luminescence intensity of Eu^{2+} in the presence of Mn^{2+}. η_T is the energy transfer efficiency from the sensitizer Eu^{2+} to the activator Mn^{2+} in $(Ca_{0.99-x}Eu_{0.01}Mn_x)_4Si_2O_7F_2$ calculated as a function of x, as shown by the black line in Fig. 4. More precisely, the η_T values were determined to be 0%, 5.87%, 13.5%, 25.3%, 32.0%, 46.3%, 66.1% and 82.3% for $(Ca_{0.99-x}Eu_{0.01}Mn_x)_4Si_2O_7F_2$ with $x = 0$, 0.005, 0.01, 0.02, 0.03, 0.05, 0.07 and 0.10, respectively. As a consequence, the energy transfer efficiency from the sensitizer Eu^{2+} to the activator Mn^{2+} in cuspidine phosphors increases gradually with increasing Mn^{2+} doping concentration. When the doped Mn^{2+} ion content was 0.1, η_T was observed to be above 82.3%.

Fig. 5 and Table 2 show the CIE chromaticity diagram and chromaticity coordinates (x, y) of the single-phase emission-tunable phosphor $(Ca_{0.99-x}Eu_{0.01}Mn_x)_4Si_2O_7F_2$ under 400 nm excitation. The chromaticity coordinates (x, y) for $(Ca_{0.99-x}Eu_{0.01}Mn_x)_4Si_2O_7F_2$ phosphors were measured to be (0.152, 0.112), (0.195, 0.191), (0.268, 0.274), (0.310, 0.288), (0.351, 0.332), (0.378, 0.366), (0.419, 0.411) eventually to (0.430, 0.423) with $x = 0$, 0.005, 0.01, 0.02, 0.03, 0.05, 0.07, and 0.1. These results indicate that the color can be tuned from blue (solely $0.01Eu^{2+}$, point 1) through white-light ($0.01Eu^{2+}$/$0.03Mn^{2+}$, point 5) and eventually to yellow ($0.01Eu^{2+}$/$0.1Mn^{2+}$,

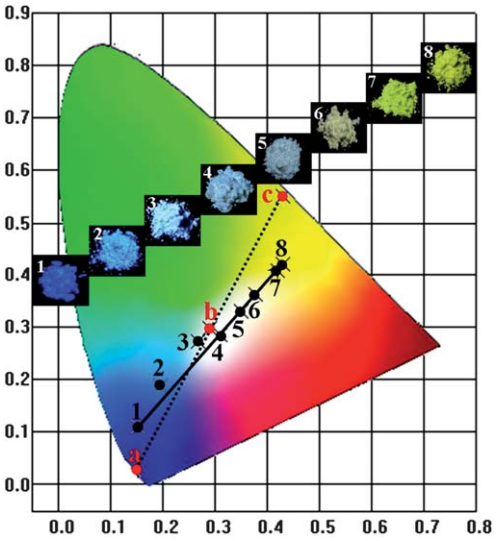

Fig. 5 CIE chromaticity diagram of $(Ca_{0.99-x}Eu_{0.01}Mn_x)_4Si_2O_7F_2$ phosphors under 400 nm excitation: (1) $x = 0$, (2) $x = 0.005$, (3) $x = 0.01$, (4) $x = 0.02$, (5) $x = 0.03$, (6) $x = 0.05$, (7) $x = 0.07$, and (8) $x = 0.1$. (a) blue InGaN chip. (b) white-light $Y_3Al_5O_{12}:Ce^{3+}$. (c) $Y_3Al_5O_{12}:Ce^{3+}$ phosphor. The insets show $(Ca_{0.99-x}Eu_{0.01}Mn_x)_4Si_2O_7F_2$ phosphors irradiated under a 365 nm UV lamp box.

Table 2 The CIE coordinates and relative emission intensity of Eu^{2+}/Mn^{2+} for $(Ca_{0.99-x}Eu_{0.01}Mn_x)_4Si_2O_7F_2$ phosphors under 400 nm excitation

CIE diagram sites	Doped Mn^{2+} molar conc.	Eu^{2+}/Mn^{2+} relative intensity	CIE chromaticity coordinates	
			x	y
1	$x = 0.000$	100/0	0.152	0.112
2	$x = 0.005$	94/16	0.195	0.191
3	$x = 0.010$	86/38	0.268	0.274
4	$x = 0.020$	75/52	0.310	0.288
5	$x = 0.030$	68/71	0.351	0.332
6	$x = 0.050$	54/78	0.378	0.366
7	$x = 0.070$	34/86	0.419	0.411
8	$x = 0.100$	18/53	0.430	0.423
a	Blue InGaN chip		0.144	0.030
b	White light $Y_3Al_5O_{12}:Ce^{3+}$		0.291	0.300
c	$Y_3Al_5O_{12}:Ce^{3+}$ phosphor		0.429	0.553

point 8) in the visible spectral region by systematically adjusting the relative Mn^{2+} dopant concentrations. The insets of Fig. 5 show photographs of $(Ca_{0.99-x}Eu_{0.01}Mn_x)_4Si_2O_7F_2$ phosphors with different Mn^{2+} contents x in a 365 nm UV lamp box.

3.3. Energy transfer mechanism and critical distance

The energy transfer mechanism for multipolar interactions has been discussed by many authors and can be determined using the relation[28]

$$\frac{I_{S0}}{I_S} \propto C^{\alpha/3} \quad (4)$$

where C is the concentration of Mn^{2+}; I_{S0} and I_S are the luminescence intensities of the sensitizer Eu^{2+} in the absence and presence of the activator Mn^{2+}. $I_{S0}/I_S \propto C^{\alpha/3}$ with $\alpha = 6$, 8, and 10 corresponds to dipole–dipole, dipole–quadrupole, and quadrupole–quadrupole interactions, respectively. The linear (red line) and polynomial (blue line) fits to the relationship between I_{S0}/I_S and $C^{\alpha/3}$ based on the above equation are illustrated in Fig. 6a–c. For Fig. 6a and c, the R^2 of the linear fit is less than that of the polynomial fit. The R^2 values for Fig. 6b of the linear and polynomial fits were calculated to be 0.9980 and 0.9964, which means that the relationship is closest to a linear behavior when $\alpha = 8$. Therefore, the energy absorbed by Eu^{2+} is transferred to Mn^{2+} *via* a nonradiative dipole–quadrupole mechanism. The above results indicate that the energy transfer occurs from the sensitizer Eu^{2+} to the activator Mn^{2+} in the $(Ca_{0.99-x}Eu_{0.01}Mn_x)_4Si_2O_7F_2$ phosphor and that the relative intensity of blue and yellow emissions can be tuned by adjusting the relative concentrations of Eu^{2+} and Mn^{2+}, respectively.

According to Dexter and Schulman,[29] concentration quenching in many cases is due to energy transfer from one activator to another until an energy sink in the lattice is reached. Blasse suggested that the critical distance R_{Eu-Mn} of energy transfer can be calculated by[30]

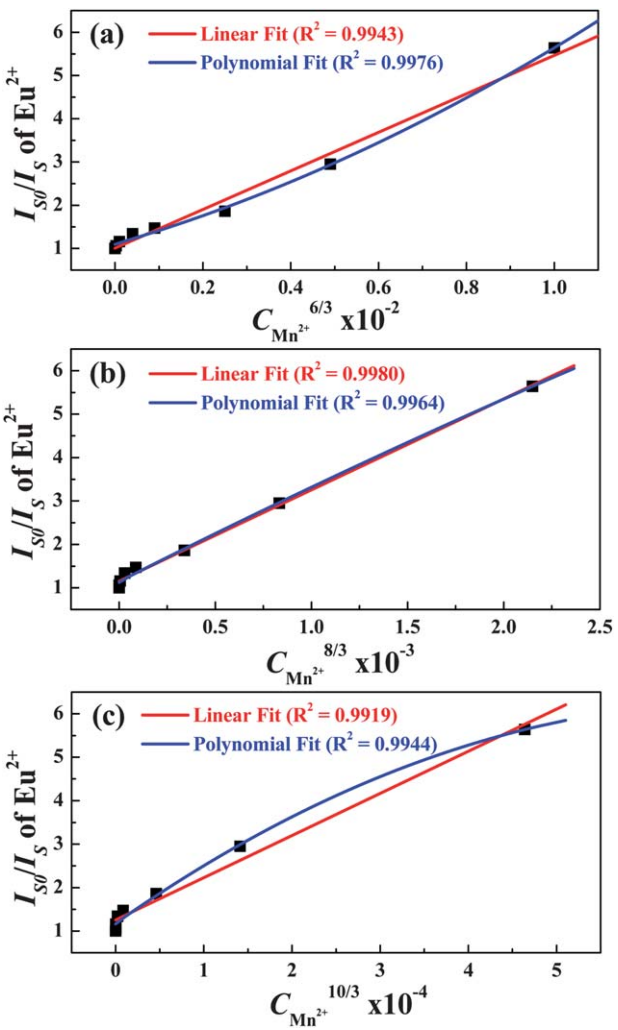

Fig. 6 Dependence of I_{S0}/I_S of Eu^{2+} on (a) $C^{6/3}$, (b) $C^{8/3}$, and (c) $C^{10/3}$.

$$R_{\mathrm{Eu-Mn}} = 2\left[\frac{3V}{4\pi x N}\right]^{1/3} \quad (5)$$

where x is the total concentration of Eu^{2+} and Mn^{2+}, N is the number of Z ions in the unit cell, and V is the volume of the unit cell. For the cuspidine crystal, the analytical and experimental values were $N = 4$ and $V = 802.92$ Å^3. Thus, the $R_{\mathrm{Eu-Mn}}$ values of $(Ca_{0.99-x}Eu_{0.01}Mn_x)_4Si_2O_7F_2$ were determined to be 18.56, 16.86, 14.73, 13.38, 11.69, 10.62, and 9.55 Å for $x = 0.005$, 0.01, 0.02, 0.03, 0.05, 0.07, and 0.1, respectively. The critical doping content x_c at which the luminescence intensity of Eu^{2+} is half that of the sample in the absence of Mn^{2+} is 0.2416 mol. Therefore, the critical distance (R_c) of energy transfer was calculated to be 11.66 Å.

According to Caldiño, the dipole–quadrupole probability (W_{sa}^{DQ}) can be given in terms of the critical distance of energy transfer from the sensitizer Eu^{2+} to the activeator Mn^{2+} as[31]

$$W_{sa}^{DQ} = \frac{3\hbar^4 c^4 f_q \lambda_s^2 Q_a}{4\pi n^4 \tau_s^0 f_d R_{sa}^8} \Omega(F_s, F_a) \quad (6)$$

where $\hbar$, c, π, and n are constants; Q_a is the integrated absorption coefficient of Mn^{2+} the acceptor; λ_s is the emission wavelength of the sensitizer Eu^{2+}; f_d and f_q are the oscillator strengths of the activator dipole and quadrupole electrical transitions; τ_s^0 is the intrinsic lifetime of the sensitizer; R_{sa} is the distance between the ions involved in the transfer and $\Omega(F_s, F_a) = \int F_s(E)F_a(E)E^{-4}dE$ represents the spectral overlap between the Eu^{2+} emission $F_s(E)$ and Mn^{2+} absorption $F_a(E)$ shown in Fig. 3a. The critical distance R_c of the energy transfer from the sensitizer Eu^{2+} to the activator Mn^{2+} is defined as the distance for which the probability of transfer equals the probability of radiative emission of Eu^{2+}, *i.e.*, the distance for which $W_{sa}^{DQ}\tau_s^0 = 1$. Therefore, R_c can be obtained from the following simplified equation:[32]

$$R_c^8 = 0.63 \times 10^{28} \frac{f_q \lambda_s^2 Q_a}{f_d E_s^4} \int F_s(E)F_a(E)dE \quad (7)$$

where $Q_a = 4.8 \times 10^{-16}$, f_d is the absorption coefficient of Mn^{2+}; $f_d = 10^{-7}$ and $f_q = 10^{-10}$ are the oscillator strengths of dipole and quadrupole electrical absorption transitions for Mn^{2+}; λ_s (in Å) and E (in eV) are the emission wavelength and emission energy of Eu^{2+} and $\int F_s(E)F_a(E)E^{-4}dE$ expresses the spectral overlap between Eu^{2+} and Mn^{2+}, which was estimated to be 5.2983 eV^{-1}. Therefore, the critical distance for a dipole–quadrupole type energy transfer was calculated to be 12.61 Å, which is similar to those obtained for (Ca, Mg, Sr)$_9$Y(PO$_4$)$_7$:Eu^{2+}/Mn^{2+} (11.09 Å)[33] and Ca$_9$La(PO$_4$)$_7$:Eu^{2+}/Mn^{2+} (11.36 Å)[34] and this result is in good agreement with that obtained using the concentration quenching method. These results imply that the emission intensity (peaking at 576 nm) of Mn^{2+} ions increases with decreasing Eu^{2+}–Mn^{2+} distance (or increasing Mn^{2+} content) until it reaches saturation. Furthermore, when the Mn^{2+} content exceeded 0.01 (*i.e.*, the Eu^{2+}–Mn^{2+} distance was shorter than R_c), the Mn^{2+} emission intensity began to decrease, which was attributed to the occurrence of energy reabsorption among the nearest Mn^{2+} ions.

3.4. EL spectrum of white-light LED lamps

To demonstrate the potential application of $Ca_4Si_2O_7F_2$:Eu^{2+},Mn^{2+} phosphors, a LED lamp was fabricated from a 400 nm NUV LED chip and a single-phase white-emitting composition-optimized $(Ca_{0.96}Eu_{0.01}Mn_{0.03})_4Si_2O_7F_2$ phosphor under a forward bias of 350 mA. The electroluminescence (EL) spectrum in Fig. 7a clearly shows a NUV band at around 400 nm, a blue-emitting band centered at 460 nm attributable to the $4f^7 \rightarrow 4f^65d^1$ transition of the Eu^{2+} ions, and yellow-emitting bands at around 576 nm that correspond to the $^4T_1(^4G) \rightarrow {}^6A_1(^6S)$ transition of Mn^{2+}. The optical properties of the white-light LED show a warm CCT of 4880 K and CIE color coordinates of (0.347, 0.338). For comparison, YAG:Ce^{3+} pumped with an InGaN blue chip was also considered, and this system was found to emit white-light with a CCT of 7272 K and CIE color coordinates of (0.302, 0.315), as shown in Fig. 7b. The insets of Fig. 7a and b show a well-packaged single-composition LED lamp and a white-light emission LED driven by a 350 mA current. These results demonstrate that our single-composition $(Ca_{0.96}Eu_{0.01}Mn_{0.03})_4Si_2O_7F_2$ phosphor-converted white-light NUV LED produced warm white-light and lower CCT values than a white-light LED fabricated with a YAG:Ce^{3+} phosphor pumped with a blue InGaN chip. Therefore, the $Ca_4Si_2O_7F_2$:Eu^{2+},Mn^{2+} phosphors are promising candidates for application in single-phase color-tunable white-light NUV LEDs.

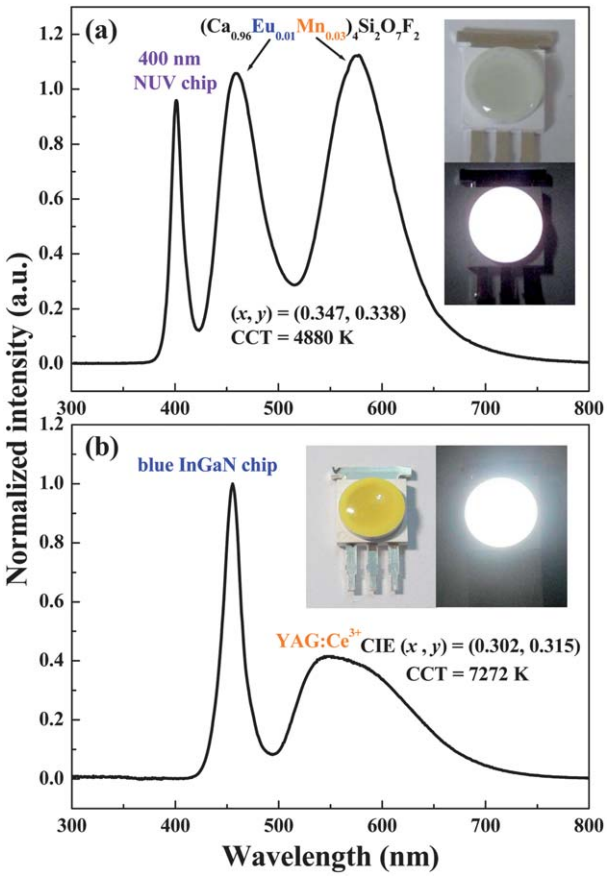

Fig. 7 EL spectrum of white LEDs fabricated using (a) a 400 nm NUV chip combined with a single-phase white-emitting $(Ca_{0.96}Eu_{0.01}Mn_{0.03})_4Si_2O_7F_2$ phosphor and (b) an InGaN chip pumped with a YAG:Ce^{3+} phosphor under a forward bias of 350 mA. The insets show photographs of the packaged white-light LEDs.

4. Conclusions

In summary, we have synthesized a series of single-composition emission-tunable $Ca_4Si_2O_7F_2$:Eu^{2+},Mn^{2+} phosphors and investigated their luminescence properties and crystal structure. We have demonstrated that the generation of white-light can be achieved using these phosphors because of the effective resonance-type energy transfer from a sensitizer Eu^{2+} to an activator Mn^{2+} *via* a dipole–quadrupole mechanism. The critical distance R_{Eu-Mn} has also been evaluated by both concentration quenching and spectral overlap methods. Because of the energy transfer, the emission hue can be varied from blue (0.152, 0.112) to white-light (0.351, 0.332) and eventually to yellow (0.430, 0.423) by tuning the Eu^{2+}/Mn^{2+} ratio. The fabricated single-phase white-light LED shows a warm white CCT of 4880 K and CIE color coordinates of (0.347, 0.338). These results indicate that our novel single-composition color-tunable $Ca_4Si_2O_7F_2$:Eu^{2+},Mn^{2+} phosphor is superior to a YAG:Ce^{3+} phosphor-converted LED pumped with a blue LED chip, which had a CCT of 7272 K and CIE color coordinates of (0.302, 0.315). Therefore, $Ca_4Si_2O_7F_2$:Eu^{2+},Mn^{2+} is a promising candidate for application in phosphor-converted white-light NUV LEDs.

Acknowledgements

This research was supported by the Industrial Technology Research Institute under contract no. B301AR4850 (C. H. H.) and in part by the National Science Council of Taiwan under contract no. NSC98-2113-M-009-005-MY3 (T. M. C.) and NSC-101-2218-E-033-001 (W. R. L.)

Notes and references

1 W. B. Im, Y. I. Kim, N. N. Fellows, H. Masui, G. A. Hirata, S. P. Den and B. R. Seshadri, *Appl. Phys. Lett.*, 2008, **93**, 091905.
2 S. Ye, F. Xiao, Y. X. Pan, Y. Y. Ma and Q. Y. Zhang, *Mater. Sci. Eng., R*, 2010, **71**, 1.
3 T. Nishida, T. Ban and N. Kobayashi, *Appl. Phys. Lett.*, 2003, **82**, 3817.
4 A. A. Setlur, W. J. Heward, Y. Gao, A. M. Srivastava, R. G. Chandran and M. V. Shankar, *Chem. Mater.*, 2006, **18**, 3314.
5 C. H. Huang, Y. C. Chen, T. M. Chen, T. S. Chan and H. S. Sheu, *J. Mater. Chem.*, 2011, **21**, 5645.
6 X. J. Wang, D. Jia and W. M. Yen, *J. Lumin.*, 2003, **102**, 34.
7 B. Lei, Y. Liu, Z. Ye and C. Shi, *J. Lumin.*, 2004, **109**, 215.
8 J. S. Kim, G. C. Kim and T. W. Kim, *Appl. Phys. Lett.*, 2004, **85**, 3696.
9 C. H. Huang, T. M. Chen, W. R. Liu, Y. C. Chiu, Y. T. Yeh and S. M. Jang, *ACS Appl. Mater. Interfaces*, 2010, **2**, 259.
10 J. S. Kim, P. E. Jeon, J. C. Choi, H. L. Park, S. I. Mho and G. C. Kim, *Appl. Phys. Lett.*, 2004, **84**, 2931.
11 S. Choi, Y. J. Yun and H. K. Jung, *Mater. Lett.*, 2012, **75**, 186.
12 Z. Xia, P. Du, L. Liao, G. Li and S. Jin, *Curr. Appl. Phys.*, 2010, **10**, 1087.
13 Z. F. Pan, C. J. Zhu, C. K. Duan, J. Xu, W. H. Liu and L. L. Wang, *J. Electrochem. Soc.*, 2012, **159**, 18.
14 Q. Ning, B. Wang, S. Gu and F. Guo, *Adv. Mater. Res.*, 2011, **239–242**, 612.
15 N. Guo, Y. Huang, M. Yang, Y. Song, Y. Zheng and H. You, *Phys. Chem. Chem. Phys.*, 2011, **13**, 15077.
16 C. H. Huang, W. R. Liu and T. M. Chen, *J. Phys. Chem. C*, 2010, **114**, 18698.
17 A. C. Larson and R. B. Von Dreele, *Generalized Structure Analysis System (GSAS)*, Los Alamos National Laboratory Report LAUR, 1994, pp. 86–748.
18 R. F. Smirnova, I. M. Rumanova and N. V. Belov, *Zap. Vses. Mineral. O-va.*, 1955, **84**, 159.
19 C. H. Huang, Y. C. Chen, T. W. Kuo and T. M. Chen, *J. Lumin.*, 2011, **131**, 1346.
20 C. C. Lin and R. S. Liu, *J. Phys. Chem. Lett.*, 2011, **2**, 1268.
21 Y. C. Chiu, C. H. Huang, T. J. Lee, W. R. Liu, Y. T. Yeh, S. M. Jang and R. S. Liu, *Opt. Express*, 2011, **19**, A331.
22 J. C. de Mello, H. F. Wittmann and R. H. Friend, *Adv. Mater.*, 1997, **9**, 230.
23 R. J. Xie, K. Kimoto, T. Sekiguchi, Y. Yamamoto, T. Suehiro, M. Mitomo and N. Hirosaki, *Appl. Phys. Lett.*, 2005, **86**, 211905.
24 R. V. S. S. N. Ravikumar, K. Ikeda, A. V. Chandrasekhar, Y. P. Reddy, P. S. Rao and J. Yamauchi, *J. Phys. Chem. Solids*, 2003, **64**, 2433.
25 W. C. Ke, C. C. Lin, R. S. Liu and M. C. Kuo, *J. Electrochem. Soc.*, 2010, **157**, J307.
26 T. W. Kuo, C. H. Huang and T. M. Chen, *Opt. Express*, 2010, **18**, A231.
27 P. I. Paulose, G. Jose, V. Thomas, N. V. Unnikrishnan and M. K. R. Warrier, *J. Phys. Chem. Solids*, 2003, **64**, 841.
28 C. H. Huang and T. M. Chen, *J. Phys. Chem. C*, 2011, **115**, 2349.
29 D. L. Dexter and J. A. Schulman, *J. Chem. Phys.*, 1954, **22**, 1063.
30 G. Blasse, *Philips Res. Rep.*, 1969, **24**, 131.
31 U. G. Caldiño, A. F. Muñoz and J. O. Rubio, *J. Phys.: Condens. Matter*, 1993, **5**, 2195.
32 J. S. Kim, K. T. Lim, Y. S. Jeong, P. E. Jeon, J. C. Choi and H. L. Park, *Solid State Commun.*, 2005, **135**, 21.
33 C. H. Huang, P. J. Wu, J. F. Lee and T. M. Chen, *J. Mater. Chem.*, 2011, **21**, 10489.
34 C. H. Huang and T. M. Chen, *Opt. Express*, 2010, **18**, 5089.

